Planetary and Space Science 58 (2010) 1139–1151

Contents lists available at ScienceDirect

Planetary and Space Science

journal homepage: www.elsevier.com/locate/pss

Day-side ionospheric conductivities at Mars

H.J. Opgenoorth [a,b,c,*], R.S. Dhillon [d], L. Rosenqvist [a,e], M. Lester [d], N.J.T. Edberg [a,d], S.E. Milan [d], P. Withers [f], D. Brain [g]

[a] Swedish Institute of Space Physics, Lagerhyddsvagen 1, Box 537, SE 751 21, Uppsala, Sweden
[b] European Space Agency, ESA-ESTEC, AG 2200 Noordwijk, The Netherlands
[c] Max-Planck-Inst. f. Sonnensystemforschung, Max-Planck-Str.2, 37191 Katlenburg-Lindau, Germany
[d] Department of Physics and Astronomy, University of Leicester, Leicester LE1 7RH, UK
[e] Försvarets Forskningsinstitut, 16490 Stockholm, Sweden
[f] Center for Space Physics, Boston University, 725 Commonwealth Ave, Boston, MA 02215, USA
[g] Space Sciences Lab, University of California, 7 Gauss Way, Berkeley, CA 94720, USA

ARTICLE INFO

Article history:
Received 29 January 2010
Received in revised form
6 April 2010
Accepted 6 April 2010
Available online 29 April 2010

Keywords:
Mars
Ionosphere
Conductivity
Induced magnetosphere
Electrodynamic coupling
Crustal magnetic anomalies

ABSTRACT

We present estimates of the day-side ionospheric conductivities at Mars based on magnetic field measurements by Mars Global Surveyor (MGS) at altitudes down to ~100 km during aerobraking orbits early in the mission. At Mars, the so-called ionospheric dynamo region, where plasma/neutral collisions permit electric currents perpendicular to the magnetic field, lies between 100 and 250 km altitude. We find that the ionosphere is highly conductive in this region, as expected, with peak Pedersen and Hall conductivities of 0.1–1.5 S/m depending on the solar illumination and induced magnetospheric conditions. Furthermore, we find a consistent double peak pattern in the altitude profile of the day-side Pedersen conductivity, similar to that on Titan found by Rosenqvist et al. (2009). A high altitude peak, located between 180 and 200 km, is equivalent to the terrestrial peak in the lower F-layer. A second and typically much stronger layer of Pedersen conductivity is observed between 120 and 130 km, which is below the Hall conductivity peak at about 130–140 km. In this altitude region, MGS finds a sharp decrease in induced magnetic field strength at the inner magnetospheric boundary, while the day-side electron density is known to remain high as far down as 100 km. We find that such Titan-like behaviour of the Pedersen conductivity is only observed under regions of strongly draped magnetospheric field-lines, and negligible crustal magnetic anomalies below the spacecraft. Above regions of strong crustal magnetic anomalies, the Pedersen conductivity profile becomes more Earth-like with one strong Pedersen peak above the Hall conductivity peak. Here, both conductivities are 1–2 orders of magnitude smaller than the above only weakly magnetised crustal regions, depending on the strength of the crustal anomaly field at ionospheric altitudes. This nature of the Pedersen conductivity together with the structured distribution of crustal anomalies all over the planet should give rise to strong conductivity gradients around such anomalies. Day-side ionospheric conductivities on Mars (in regions away from the crustal magnetic anomalies) and Titan seem to behave in a very similar manner when horizontally draped magnetic field-lines partially magnetise a sunlit ionosphere. Therefore, it appears that a similar double peak structure of strong Pedersen conductivity could be a more general feature of non-magnetised bodies with ionised upper atmospheres, and thus should be expected to occur also at other non-magnetised terrestrial planets like Venus or other planetary bodies within the host planet magnetospheres.

1. Introduction

The ionised upper atmospheres of solar system bodies can be highly conducting. In these layers, the collisions of electrons and ions with the neutral atmosphere will permit currents perpendicular to **B**, the magnetic field vector, thereby enabling the low altitude closure of magnetic field-aligned currents in the vicinity of these bodies. It is well known from terrestrial studies that such three-dimensional current systems play an important role in the global coupling of a planet to the surrounding plasma environment (e.g. Cowley, 2000) and in the control and channelling of atmospheric loss processes. The actual ability of ionospheric currents to flow perpendicular to **B** depends strongly on the

* Corresponding author at: Swedish Institute of Space Physics, Lagerhyddsvagen 1, Box 537, SE 751 21 Uppsala, Sweden. Tel.: +46 184715912.
E-mail address: opg@irfu.se (H.J. Opgenoorth).

0032-0633/$ - see front matter © 2010 Elsevier Ltd. All rights reserved.
doi:10.1016/j.pss.2010.04.004

magnitude of **B** and its variation with altitude, but does not depend on the field's origin. That is, it is irrelevant whether the magnetic field results from processes internal to the solar system body, such as a core dynamo, or the draping of field-lines around the planetary body from an external source, such as the solar wind. In the presence of a sufficiently strong magnetic field the ionospheric conductivity depends on collisions of electrons and ions with neutral particles. The result are anisotropic and dynamic ionospheric conductivities that vary with altitude, latitude and longitude, and also with time, as it depends on the solar irradiation and the solar wind conditions. The ability of the ionosphere to conduct an electrical current influences atmospheric dynamics through coupling of the plasma motion to neutral winds (ion drag) and changes the atmospheric thermal structure through energy deposition or exchange between the plasma and the neutral regimes (collisional Joule heating).

In a recent study, Rosenqvist et al. (2009) investigated the interaction between the upper atmosphere of Titan and Saturn's magnetic field and showed for the first time the altitude dependence of strong perpendicular conductivities, which exist in weak induced magnetospheres around planet-like bodies featuring a partially ionised upper atmosphere. In particular, Rosenqvist et al. (2009) found that the Hall and Pedersen conductivities in such weak draped magnetic fields can be much stronger than those observed on Earth for even the most intense substorm events driven by extreme solar wind conditions. They also found that the altitude structure of conducting layers at Titan and Earth differs. Earth has two layers, one is characterised by high Hall conductivity and the other is characterised by high ion Pedersen conductivity. Due to Earth's strong intrinsic magnetic field, a low altitude electron Pedersen conductivity does not form. At Titan, where the magnetic field in the ionosphere results from the draping of field-lines from the dipolar Kronian magnetic field, the external magnetic field strength principally decreases with decrease in altitude, and thus the electron Pedersen conductivity layer is typically not suppressed. For quite a number of Titan flybys Cassini did, however, no monotonous decline in the lower altitude B-field is observed. At such occasions layers of low altitude magnetic field, variations might indicate local ionospheric currents (Karin Ågren, IRF-Uppsala, private communication). Whatever the nature of the horizontal current systems is at Titan, it is interesting to note that closure of field-aligned currents at Titan can occur through three highly conducting ionospheric layers, which must lead to interesting and yet unknown effects in the electrodynamic coupling between the ionospheric layers themselves, and furthermore between the moon's upper atmosphere and the surrounding Kronian magnetosphere.

Inspired by the findings of Rosenqvist et al. (2009), we hypothesized that the interplay of decline in the magnetic field with decline in altitude in a region of still reasonably strong ionisation, which at Titan occurs at 1000–1400 km, was not a coincidence, but was determined by the pressure balance between the outer magnetic field pressure of the host planet and the inner ionospheric thermal pressure. In a similar way, the ionised upper atmospheres of the terrestrial planets without intrinsic magnetic fields will be partially magnetised by induced magnetospheres, created by interplanetary magnetic field (IMF) draping around the conducting obstacles. Consequently, similar conductance layers as observed on Titan should be expected at Mars.

Mars, which has recently been visited by several space missions carrying appropriate suites of plasma instrumentation, e.g. NASA's Mars Global Surveyor, MGS, (Acuña et al., 2001; Mitchell et al., 2001; Tyler et al., 2001) and ESA's Mars Express (Chicarro et al., 2004), is a natural location for a follow-up study on the general topic of ionospheric conductivities within a magnetosphere induced by the IMF draping. Numerous authors (e.g. Luhmann and Brace, 1991; Cloutier and Daniell, 1973; Brain et al., 2006a; Brain, 2006; Nagy et al., 2004) have described the induced magnetosphere of Mars, which is bounded by an outer boundary called the magnetic pile-up boundary (MPB), and an inner magnetospheric boundary, where the magnetic field declines towards the ionosphere. This induced magnetosphere is thought to result from pressure balance between the solar wind dynamic pressure, the piled-up draped solar wind IMF and the thermal pressure of the strongly ionised day-side upper atmosphere. Mars is particularly interesting as it not only features a draped induced magnetosphere through solar wind interaction but also exhibits considerable remanent crustal magnetic field pockets, which are often stronger than the induced magnetic field (Acuña et al., 1998; Acuña et al., 2001) and can even extend outside the magnetic pile-up boundary, creating a small magnetopause in the solar wind (Acuña et al., 2001 and Brain, 2006). Thus, it can be expected that the interaction of the upper atmosphere of Mars with the solar wind plasma is both Earth-like at regions of strong crustal magnetic anomalies, and Titan-like (as regards the interaction with the Kronian plasma) above the weakly magnetised surface regions.

Using mainly undisturbed night-side magnetic field measurements from MGS, Purucker et al. (2000) and Connerney et al. (2001) have derived maps of crustal anomalies over the entire planet. Such maps show that crustal fields are strongest in the heavily cratered, and thus older, southern hemisphere. Only locations of large basins, and the younger sparsely cratered northern hemisphere region (particularly in the Tharsis region and around Olympus Mons), are largely devoid of crustal anomalies.

In order to carry out a study similar to that of Rosenqvist et al. (2009) for ionospheric conductivities in the ionosphere of Mars, one would ideally need access to simultaneous measurements of both ionospheric plasma density and magnetic fields throughout the altitude regime of the Martian dynamo region. According to Withers (2009), this region should be located somewhere between 100 and 250 km altitude (see also our own observations and calculations below). Unfortunately, there has been so far no satellite at Mars, which will be able to provide both such datasets simultaneously for the same location. Therefore, studies of ionospheric conductivities must utilize models either of magnetic fields or of electron densities. Observations of the magnetic field at ionospheric altitudes were made by the MGS magnetometer during the spacecraft's aerobraking phases. Observations of ionospheric plasma densities have been made by many radio occultation experiments, including MGS (Tyler et al., 2001) and Mars Express (Pätzold et al., 2005), the topside ionospheric sounder MARSIS-AIS carried by Mars Express (Picardi et al., 2004; Gurnett et al., 2008), and in situ Viking Lander instruments (Hanson et al., 1977). Based on such data, many reasonable models of Martian day-side ionospheric plasma densities have been derived, including simple Chapman layer models (see e.g. Fox and Yeager, 2006; Gurnett et al., 2008; Withers, 2009).

The only other publication that, to the best of our knowledge, explicitly deals with day-side altitude profiles of Martian ionospheric conductivities chose to use modelled magnetic fields. Dubinin et al. (2008) investigated ionospheric conductivities, particularly in the vicinity of magnetic anomalies, in order to explain the possible existence of field-aligned currents in so-called the magnetic cusps. This work was inspired by night-side observations of field-aligned accelerated plasma by the ASPERA instrument on Mars Express (Lundin et al., 2004), and the first observation of Martian auroral emissions close to such magnetic anomalies (Bertaux et al., 2005). Dubinin et al. (2008) modelled the magnetic field as originating from a crustal anomaly,

assuming magnetic background fields of either 100 or 200 nT. They assumed the background field to be practically constant with altitude throughout the Martian dynamo region from 100 to 300 km.

This assumption was probably sufficient for the purpose of their study, but will not suffice here, as obviously the effect of crustal magnetic anomalies will decline with increase in altitude (see our discussion below in Section 3.2). They furthermore used two different representations of the electron density profiles in the near-terminator ionosphere–theoretical Chapman layer calculations and actual radio occultation result from the Viking mission. They found that the Hall and Pedersen conductivities at Mars were strong, at least an order of magnitude greater than on Earth, but they did not find a clear third electron Pedersen layer like the one found by Rosenqvist et al. (2009) on Titan. As we would like to study in particular the effects of the draped magnetosphere on the conductivities, we will therefore adopt the complementary approach of studying ionospheric conductivities over weakly magnetised crustal regions using magnetic field observations and electron density models.

2. Instrumentation and data analysis

2.1. Magnetic field data from the MGS aerobraking phase

During its two aerobraking phases in 1997 and 1998–1999, the MGS spacecraft dipped into the Martian ionosphere down to an altitude of 100 km, thus measuring the magnetic field down to very low values, which is right through the inner induced magnetospheric boundary where the piled-up magnetic field decreases towards the planet. Rosenqvist et al. (2009) used similar magnetic data from Cassini fly-by measurements at Titan. In Fig. 1, we show one of the few examples during the aerobraking phase (from 1150 to 1440 UT on September 19, 1997), when the MGS plasma package was switched on throughout the closest approach, starting and ending in the undisturbed solar wind. We use this example to illustrate the typical MGS magnetometer observations at the principal magnetospheric boundaries and regions; other data used further below will be somewhat more restricted in extent around the peri-center.

In the first and the second panels of Fig. 1, (total field $|\mathbf{B}|$ and components of $\mathbf{B}$, respectively) one can clearly recognise the undisturbed solar wind magnetic field before and after the spacecraft passes the bow-shock (BS) at 1234 UT (inbound) and 1400 UT (outbound). From 1235 to 1255 UT and from 1335 to 1400 UT, the magnetic field is seen to be turbulent, which is typical for the magnetosheath (red shading in Fig. 1). At 1255 UT (inbound), the spacecraft passes the magnetic pile-up boundary (MPB) and again at 1335 UT (outbound), thus passing for about 40 min (green shading) through a weak induced magnetosphere, draped around the day-side of Mars. Around closest approach at about 1315 UT, the draped magnetic field decreases from the relatively weak pile-up value of 15–20 nT to only 2–3 nT. However, we also note that there are at least two intense narrow spikes in $|\mathbf{B}|$ around the location of the closest approach, which are of the order 10 nT. For comparison we have plotted the corresponding $|\mathbf{B}|$ value of crustal magnetic field from the Cain model (Cain et al., 2003) in the third panel. We have then tried to subtract the total magnetic field from the Cain anomaly model (calculated for orbit altitude) from the measured MGS magnetic field, illustrated in the 4th panel, which gives the "residual" induced field $|\mathbf{B}|_{res} = |\mathbf{B}_{measured} - \mathbf{B}_{Cain}|$.

However, such simple subtraction was not very successful in cleaning the external magnetic data from the internal components. All we can deduce in this case is that the Cain model does not exactly reproduce the spikes seen in the data, and also

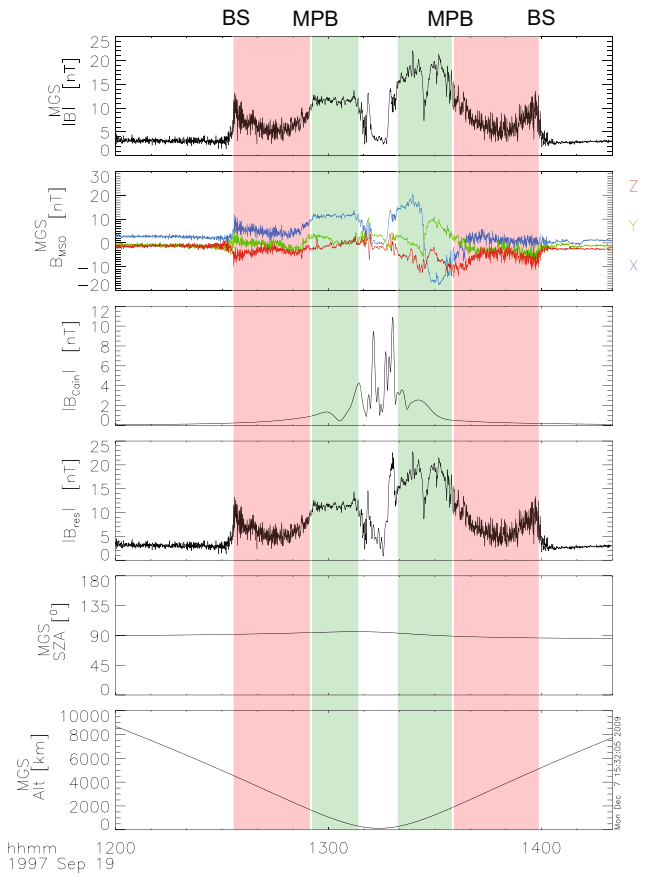

Fig. 1. MGS data around peri-center approach for September 19, 1997, 1200–1420 UT. The panels show from top to bottom the total magnetic field B_{total}, the component magnetic field in Mars Sun orbital (MSO) coordinates (*X*-blue, *Y*-green and *Z*–red,) the magnetic field B_{Cain} at orbit altitude according to the model by Cain et al. (2003), the residual field $B_{total} - B_{cain}$, the Solar zenith angle (SZA), and the altitude of MGS. Note that in this case the draped magnetic field is weak, about twice the strength of the crustal magnetic field from below. The crossings of the bow-shock and the magnetic pile-up boundary are marked with BS and MPB, respectively, and the magnetosheath and magnetosphere regions are shaded in red and green, respectively.

appears to have some kind of latitudinal offset for the major two spikes. Of course we should recognise that the model has been based on heavily averaged MGS data and probably does not help very much to derive the magnetic effects of a cleanly draped external magnetosphere from the MGS orbital data. Thus we decided for this study to use only MGS data from orbits where the ratio between the strength of the draped magnetospheric field and the local crustal magnetic anomalies from below was large enough for the latter to be neglected. For later reference it should be noted that panel 5 in Fig. 1 shows the solar zenith angle (SZA) variations along the orbit.

In this paper, we want to study initially only the cases with a clear decline of the magnetic field strength at ionospheric altitudes above regions of negligible crustal fields. Therefore, we selected by visual inspection 10 out of several hundred aerobraking orbits as being minimally affected by crustal magnetic fields. Fig. 2 illustrates such a low peri-center data example on October 4, 1998, from about 1600 to 1930 UT, where the closest approach of 100 km occurred at 1745 UT. In this case, the crustal magnetic field according to the Cain model (third panel, localised maximum of about 10 nT) is by a factor of 7–8 weaker than the draped external magnetospheric $|\mathbf{B}|$ of almost 80 nT (top panel). In contrast to Fig. 1, the data during this orbit do not extend from the solar wind to the solar wind outside the

bow-shock; however, in analogy we can clearly identify the passages into and out of the MPB (around 1735 and 1755 UT, respectively), and the decline in the draped magnetic field strength just before and after the closest approach. For all 10 selected orbits, we found principally similar magnetic field decline features around peri-center, although the peak magnitude of the draped magnetic field varied between the individual orbits from 30 to 90 nT, obviously due to the prevailing solar wind conditions within this set of 10 orbital timeslots. It is also possible that the location of the low altitude portion of the orbit with respect to the actual draping geometry might have affected the observed magnetic field intensity.

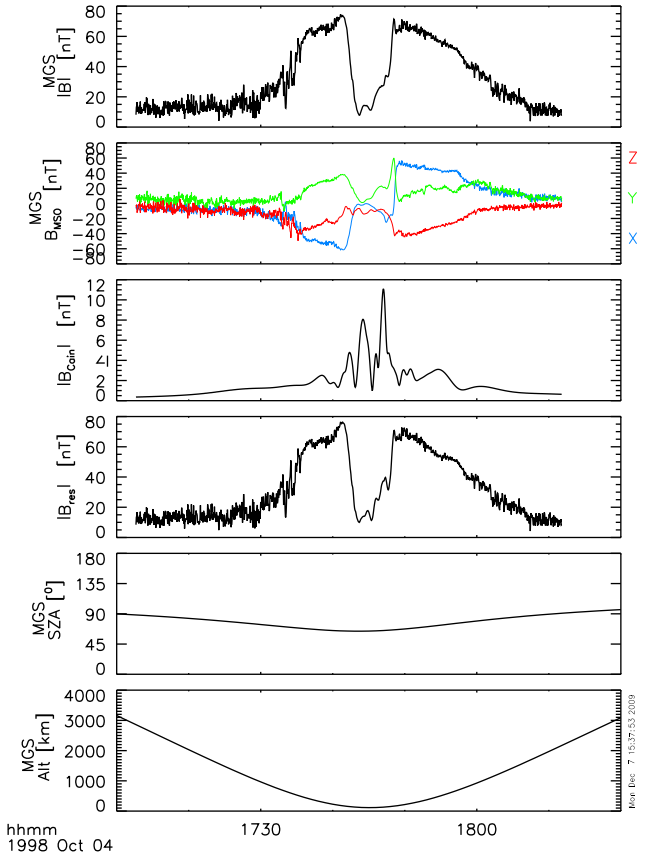

Fig. 2. Same format as Fig. 1, but for a selected orbit (no 1 in Table 1), exhibiting strongly draped magnetic fields with peri-center closest approach over a region with weak crustal magnetic fields (about 15% of the induced magnetospheric field).

Inspecting the ground tracks of the selected orbits, we found that all 10 peri-center approaches fall into the northern hemisphere, and 8 of them just to the north of the Tharsis region near Olympus Mons, an area which is known to be free from major magnetic anomalies (Connerney et al., 2001). Fig. 3 shows the MGS ground track for 15 min around the peri-center for the 10 orbits used in this study (labelled 1–10) superimposed on a map of the modelled effects of crustal magnetic fields at 200 km altitude (Purucker et al., 2000). The 15 min duration of the ground tracks is chosen to ensure that the parts of the orbit with altitudes lower than 300 km are represented, i.e. we should cover the track through the dynamo region, which is discussed extensively further below. Table 1 lists the dates and times of the closest approach and orbit numbers for all selected orbits for possible future reference and identification.

Since the Martian crust is probably full of scattered small magnetic anomalies, it is difficult for an orbiting satellite to stay above regions where the decline in the magnetic field strength at the inner magnetospheric boundary is undisturbed for long periods. Nevertheless, we think that we can safely assume that in our selected cases the gross features of large scale increase and decline in the observed magnetic field due to altitude variations in the draped magnetosphere. Thus we constructed from each of the ten orbits vertical profiles of magnetic field strength for the inbound and outbound legs, as illustrated in Fig. 4 (for the same data as in Fig. 2, Orbit 1 in Fig. 3). Here, the red curve represents the magnetic variations with altitude from the inbound leg and the green curve from the outbound leg. From Fig. 3, we see that the region throughout the Tharsis Montes, where this orbit's periapsis occurred, is free from significant crustal field anomalies, and thus we can assume that the variations that we see stem mostly from the, at first approximation, horizontal layer of draped external field. Thus the presentation of the observed field as a function of altitude in Fig. 4 should come very close to the true vertical profile of $B(h)$ in this region despite the large horizontal extent of the measurements.

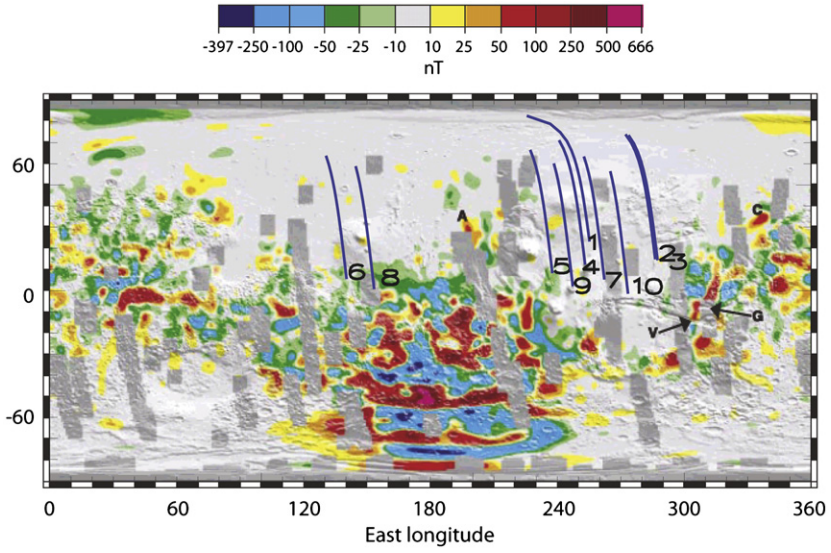

Fig. 3. Map of the crustal anomalies over the Mars surface, normalised for the magnetic field strength seen at 200 km altitude (from Purucker et al. 2000). Within this map, we show the ground projection of the MGS orbit for 15 min around each peri-center (for orbit altitudes below 300 km) for 10 selected orbits. The numbering is according to the list of selected orbits in Table 1. (Please note that arrows and other letterings stem from the original reference and have no meaning here).

Table 1
List of selected MGS orbits.

#	Date	Time (UT)	Orbit
1	04-10-1998	1710–1820	0597
2	25-10-1998	0350–0440	0649
3	26-10-1998	0410–0520	0652
4	31-10-1998	0940–1050	0668
5	08-11-1998	1540–1650	0696
6	08-11-1998	2220–2330	0697
7	11-11-1998	1600–1700	0707
8	15-11-1998	0120–0230	0720
9	15-11-1998	1930–2040	0723
10	17-11-1998	1900–2010	0731

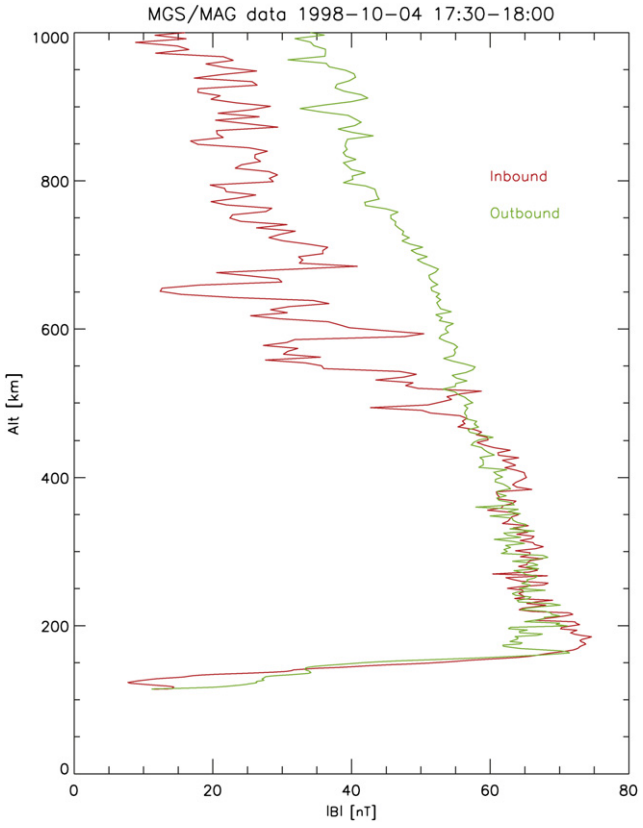

Fig. 4. Same data as top panel in Fig. 2, total magnetic field, as measured by MGS around peri-center, plotted against altitude for the inbound (red) and outbound (green) leg. Note that the closest approach of MGS is at 100 km altitude. For interpretation of the references to colour in this figure legend, the reader is referred to the web version of this article.

The slight difference between the vertical profiles obtained from the inbound and outbound legs appears to stem from differences in draping geometry as earlier pointed out by Bertucci et al. (2003) and Edberg et al. (2008). We see the MPB being clearly defined above around 500 km on the inbound leg, which is closest to the sub-solar point and has relatively small SZA; yet, there is somewhat more flaring on the outbound leg, which is closest to the terminator and has relatively large SZA. As our study deals entirely with the magnetic field profile around the dynamo region from 100 to 300 km altitudes, these, mostly high altitude differences, are not relevant for our results (see altitude range of Figs. 5–9 below). This orbit has been particularly chosen to illustrate that even an apparently uniformly draped induced magnetosphere can be slightly non-spherical, but also that this non-sphericity has negligible effects for the principle results of our study.

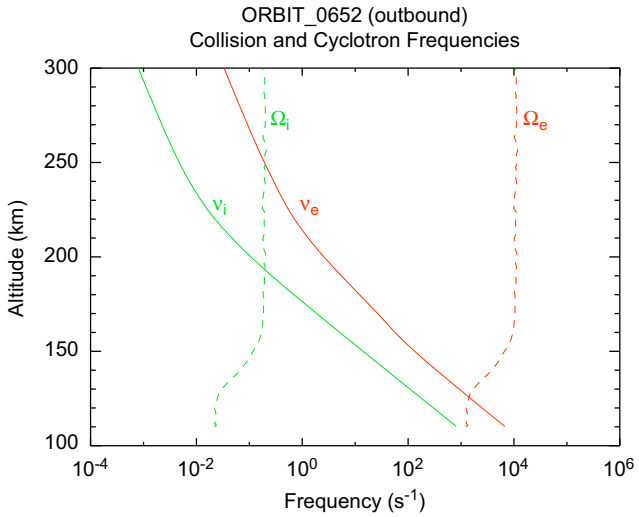

Fig. 5. Collision (solid lines) and gyro-frequencies (broken lines) for ions and electrons versus altitude, based on the assumptions given in the text and using the magnetic field data shown in Fig. 4. The dynamo layer at Mars is defined by the altitude region between the two crossing points where $\Omega_i = \nu_i$ (upper region) and $\Omega_e = \nu_e$ (lower region).

Next we determined the appropriate electron density profiles in the day-side hemisphere. Thousands of electron density profiles from radio occultation experiments and several years of Mars Express topside sounder data have shown that – throughout the entire day-side – the region near the main peak of the Martian ionosphere behaves according to Chapman theory (Gurnett et al., 2007; Withers, 2009). This means that the intensity and peak altitude of the ionisation maximum can be represented as depending mostly on SZA. Of course, it is well known that, particularly close to the terminators where most of the occultation profiles have been acquired, there often exists a small lower layer of ionisation, at around 110 km altitude (see e.g. Fox and Yeager, 2006, Withers, 2009, and references therein). This so-called the M1 layer is typically explained by ionisation through secondary energetic electrons, caused in the lower ionosphere by solar X-ray radiation. This layer is typically seen as a small "knee" in the bottom end of the larger Chapman-type M2 layer at 140–150 km altitude, which is caused by direct photo-ionisation. In our case, it would be very hard to include an M1 layer model due to the absence of information on the Solar X-ray radiation at Mars. We felt confident to calculate ionospheric conductivities in regions outside the crustal magnetic anomalies on the basis of theoretical Chapman layer ionisation profiles (for the appropriate SZA illumination) and measured magnetic fields throughout the altitude range of the Martian dynamo region, in particular, as our results on particular altitude structures in the conductivities turned out to be robust even with the simple assumption of a Chapman electron density layer (see further discussion below in Sections 3 and 4).

2.2. Anisotropic ionospheric conductivities

As already elaborated by Rosenqvist et al. (2009), the ability of any weakly ionised gas (e.g. in a planet's ionosphere) to conduct an electric current across **B** is given by the expressions for the Pedersen, Hall and field-aligned conductivities (see Boström (1964), or for a more general and more recent approach also see Withers (2008))

$$\sigma_p = \frac{en_e}{|\mathbf{B}|}\left[\frac{\Omega_e \nu_e}{\Omega_e^2+\nu_e^2}+\frac{\Omega_i \nu_i}{\Omega_i^2+\nu_i^2}\right] \quad \text{Pedersen conductivity}$$

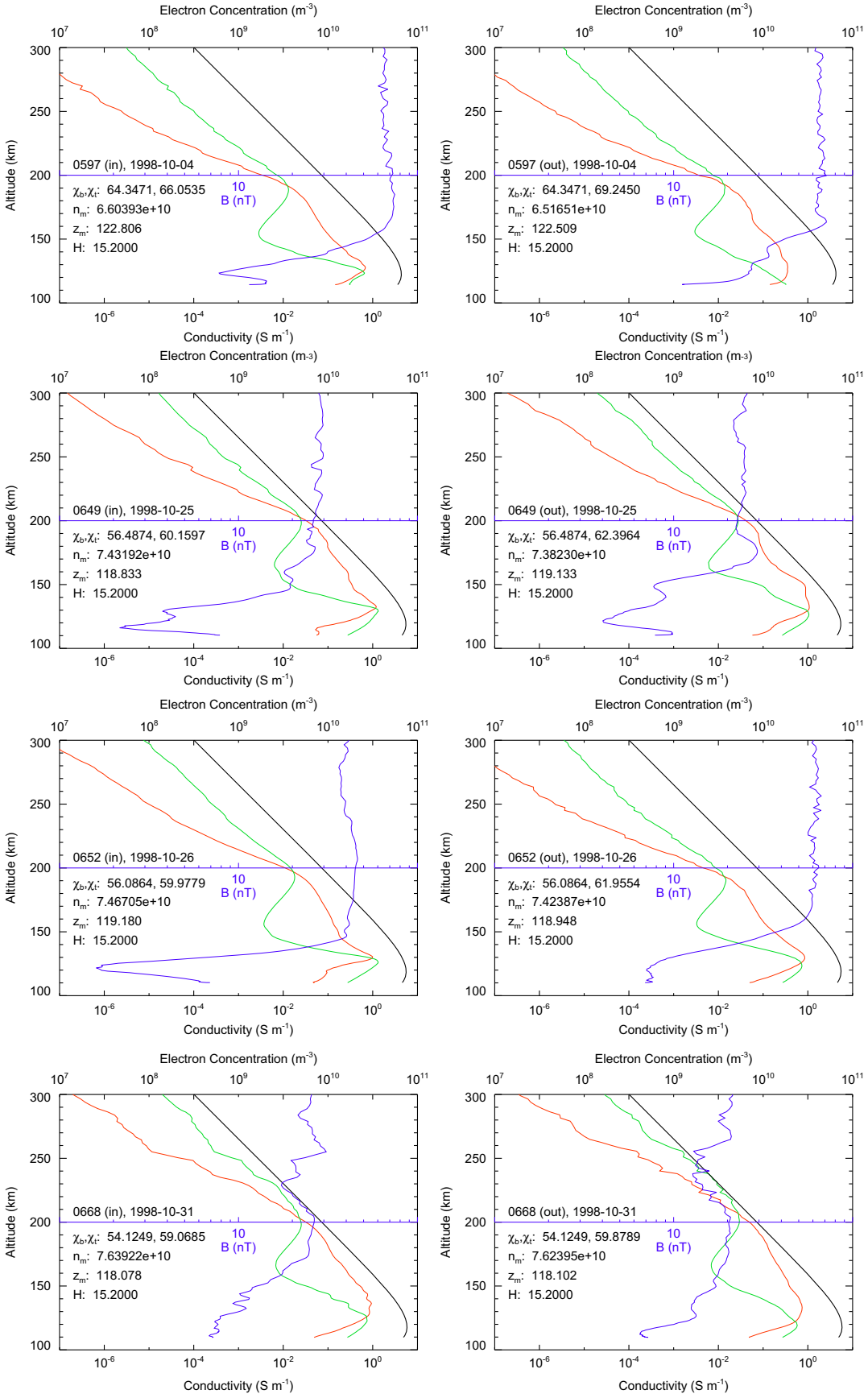

Fig. 6. Altitude profiles of measured magnetic field (blue), calculated Chapman layer profiles of electron density according to the prevailing SZA along the orbit track (black), and ionospheric conductivities, Hall (red) and Pedersen (green), for the first four of the ten selected orbits for this study (left panels inbound legs, right panels outbound legs). The labels in the panels refer to orbit number and date, SZA at peri-center and exit from the ionosphere ($_b$ and $_t$, respectively), the maximum electron density (n_m), its altitude (z_m) and the atmospheric scale height (H) used for the calculations of the conductivities. For interpretation of the references to colour in this figure legend, the reader is referred to the web version of this article.

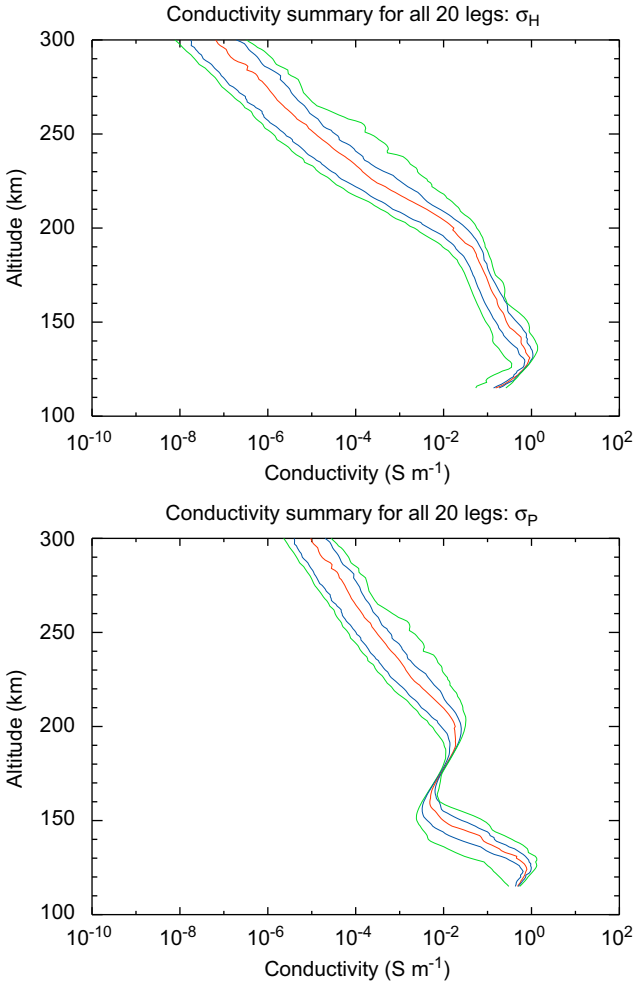

Fig. 7. Percentiles of the conductivity profiles for all ten selected orbits in this study. Using both the inbound and outbound legs, we included 20 profiles of Hall (upper panel) and Pedersen conductivities (lower panel). The minima and maxima of the curve-envelopes are indicated by green bounding lines, the quartiles with blue lines and the median value with a red line. For interpretation of the references to colour in this figure legend, the reader is referred to the web version of this article.

$$\sigma_H = \frac{en_e}{|\mathbf{B}|}\left[\frac{\Omega_e^2}{\Omega_e^2+\nu_e^2}-\frac{\Omega_i^2}{\Omega_i^2+\nu_i^2}\right] \quad \text{Hall conductivity}$$

$$\sigma_{||} = e^2 n_e\left[\frac{1}{m_i\nu_i}+\frac{1}{m_e\nu_e}\right] \quad \text{field-aligned conductivity}$$

where e is the elementary charge, m_e the electron mass, m_i is the ion mass, n_e is the electron density, and $|\mathbf{B}|$ is the magnetic field magnitude. The ion and electron gyro-frequency, respectively, are calculated as $\Omega_{i;e}=e|\boldsymbol{B}|/m_{i;e}$ and $\nu_{i;e}=\Sigma_n\nu_{in;en}$ are the ion–neutral and electron–neutral collision frequencies. The principal neutral atmospheric constituent in Mars' atmosphere below 200 km is CO_2, but above 200 km it is rather O (Chen et al., 1978), which has been accounted for in our calculations below. The main ionospheric ion is considered to be O_2^+, which is dominant at altitudes up to at least 300 km, the upper limit considered in this study (see Withers, 2009). Thus $m_i=32m_p$ where m_p is the proton mass.

We assume that collisions between the charged particles (electrons and ions) and the neutral constituents of the atmosphere of Mars are predominantly elastic, so inelastic collisions can be neglected. The elastic ion–neutral collision frequency can be approximated by

$$\nu_{in} = 2.6\times10^{-9} n_n (a_0/m_A)^{1/2} s^{-1},$$

where n_n is the neutral number density in cm^{-3}, μ_A is the ion–neutral reduced mass in atomic units and α_0 is the atomic polarizability in units of $10^{-24}\,cm^{-3}$ ($\alpha_0=2.63$ for CO_2 and $\alpha_0=0.79\pm0.02$ for O (Banks and Kockarts, 1973)). The electron–neutral collision frequency for momentum transfer is given by $\nu_{en}=5.4\times10^{10}\, n_n\sqrt{T_e}\, s^{-1}$ (T_e in K) (Kelley, 1989). Following Chen et al. (1978) and Schunk and Nagy (2000), we have used an altitude profile for T_e, which starts at 200 K at 100 km and then increases to 3000 K at about 250 km.

2.3. Calculations of conductivities

We first derived the altitude profiles of electron and ion gyro and collision frequencies according to the above equations and assumptions. Fig. 5 shows the resulting electron and ion gyro-frequencies versus the altitude in comparison to the electron–neutral and ion–neutral collision frequencies. Again, and as already pointed out in the study by Rosenqvist et al. (2009), the main difference from Earth is that the decrease in magnetic field at the inner magnetospheric boundary results in decrease in gyro-frequencies for both species. This can be understood as an effect that actually raises the altitude of, in particular, the lower portion of the dynamo layer with respect to where it would be in an Earth-like case with constant $B(h)$.

In Fig. 5, we note from the crossing points of Ω and ν for each particle species that the dynamo region at Mars (above regions of weakly magnetised crustal anomalies) is located between 100 and 200 km, in agreement with Withers (2008). The region of electron Pedersen conductivity should occur around 120–130 km altitude where $\Omega_e=\nu_e$. As in the case of Titan, and in contrast to the situation on Earth, the relatively weak magnetic field in a region of considerably ionised atmosphere indicates that this layer may be strong.

We then calculated the ionospheric conductivities using vertical profiles of the magnetic field measured by MGS and vertical profiles of electron density from a model Chapman layer. We considered a vertical range from 100 to 300 km for the 10 selected orbits, i.e. 20 legs, and used a sub-solar peak electron density of $1.0\times10^5\,cm^{-3}$, a sub-solar peak altitude of 110 km and neutral scale height of 15.2 km in the Chapman model. These values were derived from the sub-solar parameters used in the Chapman layer fit to Mars Express MARSIS data by Gurnett et al. (2008). For the calculation of the local ionisation profile, we used the real SZA along the orbit; thus it varied slightly throughout descent and ascent. For the purpose of this paper, we ignored possible variations of the solar $F_{10.7}$ irradiation from one event to the other.

3. Results

3.1. Results for day-side conductivities above weakly magnetised crustal regions

In Fig. 6, we summarise the results of our calculations by showing for the in- and outbound legs of the first four orbits (i.e. 8 profiles): the measured magnetic field, the calculated electron densities, and the resulting conductivities versus altitude. This figure clearly shows that the resulting conductivity profiles are qualitatively similar in shape from event to event, despite variability in the total induced magnetic field and the particular decline in the magnetic field strength towards lower altitudes (blue curves.) Just like Rosenqvist et al. (2009) found on

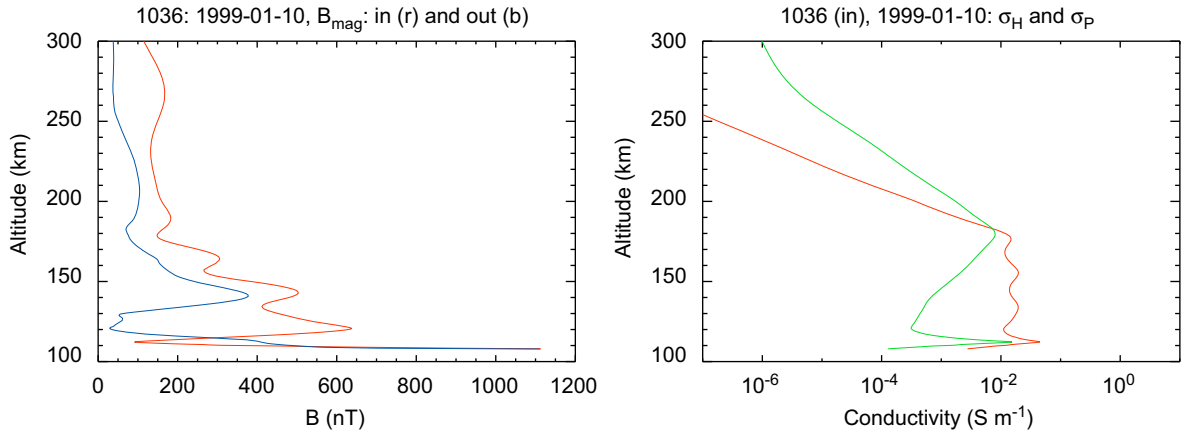

Fig. 8. Constructed altitude profiles of magnetic field (left panel) and Hall (red), Pedersen (green) and parallel conductivities (blue) (right panel) from data along the pericenter approach of orbit 1036, on January 10, 1999 (inbound leg red, outbound leg blue) crossing over a number of large crustal anomalies, resulting in an increase in the magnetic field with decrease in altitude. It clearly suffers from a strong variability introduced by latitudinal variations rather than altitude variations. The correspondingly calculated conductivities for the inbound leg in the top right panel are therefore unphysical. For interpretation of the references to colour in this figure legend, the reader is referred to the web version of this article.

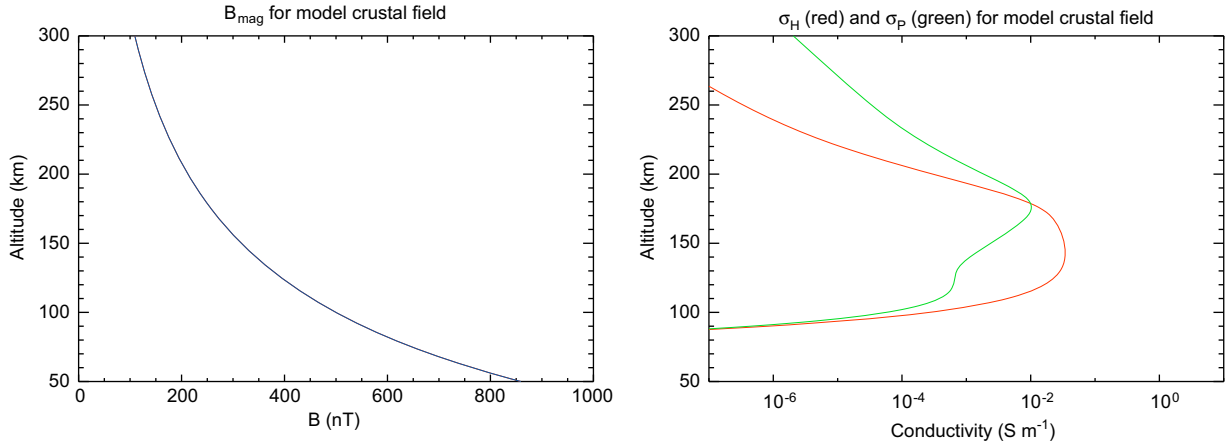

Fig. 9. Realistic model of a magnetic field altitude profile above a crustal anomaly, decreasing with an r^{-3}-dependence, where r is the distance to a buried crustal dipole (left panel). Consequently, the conductivities in the right panel can be considered to be representative for such a location.

Titan – and in contrast to Earth and the results of Dubinin et al. (2008) for strong crustal field regions on Mars – there are two distinct layers of Pedersen conductivity (green curves), one above and one below the main, somewhat structured Hall conductivity layer (red curves) in all 8 cases. If one compares the peak altitudes of the two Pedersen layers with the locations of Ω- and ν-curve crossing points for ions and electrons in Fig. 5, and also inspects the equations for σ_P and σ_H in Section 2.2 above, it becomes obvious that the upper part of the Pedersen conductivity profile stems from the restricted gyro-motion of the ions. Incomplete gyrations of ions due to collisions with neutrals lead to an average ion motion into the direction of any applied electric field **E**, and thus a relative motion of these ions with respect to the still undisturbed $\mathbf{E}\times\mathbf{B}$ drifting electrons. This feature, well known from Earth, is also the reason for a relative delay of the ion-drift with respect to the electron drift in the other perpendicular (Hall direction), and thus conductivity in the $\mathbf{E}\times\mathbf{B}$ direction. The more restricted the ion gyration becomes with decreasing altitude, in this case around 150 km, the more effective the Hall conductivity becomes in the direction perpendicular to any electric field.

At even lower altitudes, the ions will basically be tied to the motion of the neutrals, while increase in collisions with neutrals at these altitudes will even force the electrons to conduct incomplete gyration orbits, leading to a net current (conductivity) in both the Pedersen and Hall directions. This effect, which according to Figs. 5 and 6, occurs on Mars at around 120 km, and is usually suppressed on Earth by lack of ionisation at equivalent altitudes.

Fig. 6 illustrates furthermore that the variations in solar zenith angle between the selected orbits were found to be very small, and thus there is only a very small variability in both the peak value and altitude of the model electron density profile (black curves). Note however, that we have not considered changes in the solar irradiation for these curves, as we are only interested in the principal existence of various layers and not their exact altitude or detailed amplitude.

We also conclude from Fig. 6 that it was not necessary to include a small M1 layer around and below 110 km in our model electron density profiles. Such a layer is reported by e.g. Fox and Yeager (2006) and Withers (2009) to exist with varying intensities throughout the day-side ionosphere. We see now that the formation of a lower (electron-) Pedersen layer at 120 km is clearly not dependent on an additional ionisation source and a structured electron density in this region—solar photo-ionisation is fully sufficient to create such a layer in the conductivity.

On the contrary, we find that it would have been difficult to demonstrate this more general situation, if we had, indeed, attempted to include a small "knee" or extra layer in the electron

density profile close to the crucial altitude region at 110 km. Based on the results shown in Fig. 6, we can safely conclude that the electron Pedersen layer is a robust feature caused by the decline in magnetic field strength with decline in altitude, depending only on the availability of sufficient electron density at 120 km altitude. Any extra small layer of electron density at or below 110 km, i.e. at the bottom end of our basic model Chapman profile, would most probably further enhance the resulting electron Pedersen conductivity layer, but not originally cause it. Alternatively, it might for some orbits fall into an altitude region of negligible magnetic field, and thus create no noticeable conductivity enhancement. The same should be true for an even lower electron layer of possibly meteoric origin, which has recently been identified by Pätzold et al., (2005) below 100 km. It would have no impact on our conductivity profiles, but is rather expected to be efficient in the absorption of radio waves in the Martian ionosphere (see e.g. Nielsen et al., 2007a).

Inspecting Fig. 6 in more detail, we can identify clear differences in intensity and altitude dependence between the resulting conductivities of these 8 examples. As all other parameters are basically close to constant within our calculations, we conclude that the differences are due to the strength of the induced magnetosphere, and in particular, the structure of its decline with altitude at its inner boundary. This effect becomes clear if one compares the inbound legs of orbits 0597 and 0649, (top and second left panels of Fig. 6). Clearly, there is a difference in the strength of the draped magnetic field at 170–300 km altitude (70 and 25 nT respectively), and the upper Pedersen conductivity peak turns out to be larger for the event with the weaker draping. In a similar way, the very sharp decline in the draped magnetic field at the inbound leg of orbit 652 (Fig. 6, third panel on the left) results in the strongest electron Pedersen layer in these examples. In contrast, e.g., the outbound leg of orbit 597 (Fig. 6, top right panel) exhibits only a slow decline in B, resulting in a relatively small electron Pedersen layer at a very low altitude.

In order to illustrate the range of such variability in our dataset, we show in Fig. 7 the percentiles of the resulting conductivity profiles from all 20 vertical profiles used for this study. First it is clear from this figure that the double peaked nature of the Pedersen conductivity is a robust feature—a new finding of this work for Mars in contrast to Earth, but in good agreement to what Rosenqvist et al. (2009) found on Titan. There also appears to be some distinct new structure in the distribution of Hall conductivity around and below 150 km. The conductivity does not decrease immediately after the indication of a maximum below the upper Pedersen conductivity maximum, but continues to increase to a new maximum somewhat above the lower Pedersen conductivity maximum. This feature is also visible in the individual Hall conductivity profiles of Fig. 6. Again inspecting the equation for the Hall conductivity in Section 2.2 appears that this effect stems from the combination of electron and ion effects, and thus results in an altitude profile different from the terrestrial situation.

The peak values observed are about 3 S/m for both the lower Pedersen and the Hall conductivity, and about 0.05 S/m for the upper Pedersen peak (Fig. 7). At most altitudes, the variability in both conductivities is about one order of magnitude. In the discussion of Fig. 6 above, we have concluded that this variability stems mainly from the shape of the magnetic field altitude profile. However, again we note here that we have reduced the variables, which influence the electron density profile to the SZA only. This assumption, which is probably reasonably correct for the day-side ionosphere and sufficient for the purpose of this study, was chosen to demonstrate the dependence of the conductivities on the altitude profile of the magnetic field in particular. The special situation on Mars – just like on Titan and completely unlike Earth – is that on the day-side of the planet, where the variability of the ionisation of the upper atmosphere is small, the actual shape of the induced magnetosphere, and thus the state of magnetic field draping around the planet has a direct influence on the ionospheric conductivities.

3.2. Results for day-side conductivities above strong crustal anomalies

In Section 4 we will come back to these issues, which are probably valid for all solar system bodies with draped induced magnetospheres and an ionisable atmosphere. In the meantime, and as we deal with Mars in this study, we would like to discuss first the influence of the Martian crustal magnetic fields on the day-side distribution of ionospheric conductivities (and possible three-dimensional current geometries in consequence).

Dubinin et al. (2008) have shown that the ionospheric conductivity around the terminator region and above strong crustal anomalies is not unlike the terrestrial situation, with only two main conductivity layers. In the sections above, we analysed data from carefully selected orbits away from such anomalies. Consequently, we have been able to compare our results to those found in analogous situations on Titan. In this section, we contrast our results above with what one would expect to happen to day-side ionospheric conductivities above strong magnetic anomalies. At first we inspected the MGS magnetometer data from aerobraking passes over strong anomalies, but soon we realised that the horizontal gradients in the data were so large that one could not construct a meaningful vertical profile of magnetic field strength over any local anomaly. For most aerobraking passes over strong crustal anomalies, MGS passed through complicated magnetic structures resulting from several adjacent magnetic anomalies and intermediate so-called the magnetic cusps (see e.g. Gurnett et al. (2008) or Brain et al. (2007) for possible magnetic topologies). Fig. 8 (left panel) illustrates what such a false magnetic altitude profile would look like—in contrast to our examples from "clean" regions in Figs. 4 and 6 above. Consequently the results for conductivity profiles in Fig. 8 (right panel) are certainly completely meaningless, as they are not representative altitude profiles for any one location, but contain magnetic variations from longitudinal structures.

In order to overcome this problem and to improve on the results of Dubinin et al. (2008), we assumed (in accordance with other studies, e.g. Purucker et al., 2000) that the crustal anomalies can be represented as an ensemble of buried dipoles. In this way, the magnetic field seen by a descending satellite over a reasonably strong and localised anomaly should look like a field that increases with an r^{-3}-dependence, where r is the difference between the satellite's altitude and the dipole's burial depth (see a more detailed discussion in Brain et al., 2003). In the left panel of Fig. 9, we show such a synthetic, yet plausible, altitude profile of the magnetic field above a typical anomaly. In Fig. 3, the chosen example would range in the clear red or clear blue colour scale, corresponding to a magnetic field strength of ca. 200 nT at 200 km altitude. In the right frame of Fig. 9, we see the resulting altitude profiles for Hall, Pedersen and parallel conductivities for such a magnetic field situation. For simplicity, we assumed the profile to be in the sub-solar region with a SZA of 0°. Here we only want to illustrate the effect of a plausible magnetic altitude profile over a crustal anomaly on the shape of the conductivity altitude profile, and not the exact location of the maxima for any really existing anomaly. We see immediately that over such anomalies, the conductivities behave in a very Earth-like way, with one dominating Pedersen conductivity layer at the ion regime altitude and a lower stronger Hall layer. There is a slight indication for the

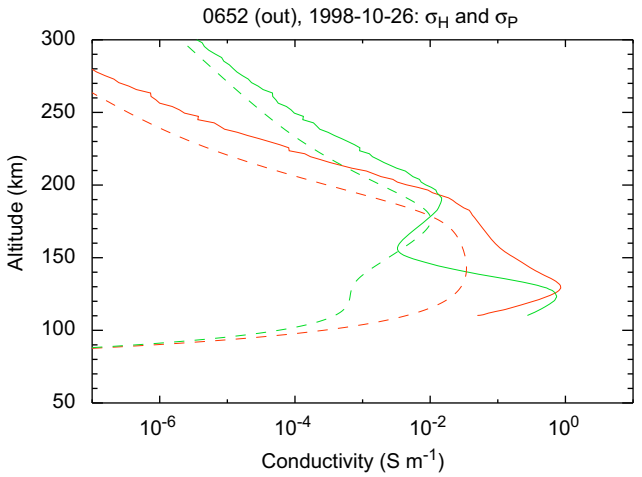

Fig. 10. Superimposed conductivity profiles for Hall and Pedersen conductivities (solid red and green curves, respectively) for the outbound leg of the quiet orbit 652 on October 26, 1998 (compare Fig. 6, third panel on the left), and the conductivities resulting from a model magnetic field over a crustal anomaly (broken red and green lines for the Hall and Pedersen conductivities, respectively; from Fig. 9, right panel). For interpretation of the references to colour in this figure legend, the reader is referred to the web version of this article.

existence of a lower electron Pedersen layer—probably because the magnetic field strength at Mars, even above crustal anomalies, is so much weaker than that on Earth, so that electron effects are not completely suppressed.

Another observation in Figs. 8 and 9 is that the overall conductivities are not only different in structure from the cases discussed so far (away from crustal anomalies), they are also much weaker—about an order of magnitude for the peak Hall and Pedersen conductivities (somewhat more for the Hall peak and somewhat less for the upper Pedersen peak), and well over two orders of magnitude in the altitude region of the absent lower layer of Pedersen conductivity. We illustrate this fact in Fig. 10, which is a superposition of the results for Hall and Pedersen conductivities above a typical strong crustal anomaly (broken lines) and below a horizontally draped magnetosphere (solid lines) only. We conclude, in agreement with other findings concerning the solar wind interaction on Mars (e.g. Brain, 2006), that even in terms of ionospheric conductivities the Martian ionosphere behaves both in Earth-like ways, in regions of strong magnetic anomalies, and in Titan-like ways in regions of draped magnetic fields outside these anomaly regions. This result explicitly implies that very strong conductivity gradients must exist in regions where these two regimes meet—a situation, which is unlikely to occur on any other solar system body.

4. Discussion

4.1. Ionospheric conductivities in the day-side magnetically undisturbed regions of Mars

Using unique data very close to and even within the Martian upper atmosphere from the MGS aerobraking phases in 1997/98, we are able to study the distribution of ionospheric conductivities in the partially magnetised ionosphere. As we had expected from the study by Rosenqvist et al. (2009) on Titan, the geometry of a draped magnetosphere facilitates the formation of three intense layers of conductivity even at Mars. This is in contrast to the well-known and well-studied situation at Earth, where conductivities due to incomplete electron gyro-motions are negligible, and thus a lower Pedersen conductivity layer does not exist. The resulting Hall and Pedersen conductivities at Mars were found to be even stronger than those on Titan, which were already one order of magnitude stronger than the most extreme cases seen on Earth.

This should imply that any applied electric field should be able to drive intense horizontal currents very effectively. Such electric fields could stem not only from either vertical or horizontal atmospheric motion or winds but also from solar wind induced convection. Whatever the mechanism, it would probably result in a current system very much like the equatorial electrojet on Earth (e.g. Egedal, 1947), but covering most of the day-side magnetosphere, with one major difference: Not only can and will the applied electric field and atmospheric winds vary depending on their respective driving forces, but also the conductivities themselves are strongly coupled to the solar wind forcing, through their dependence on the magnetic field draping.

We can clearly see this in the examples in Fig. 6 and are following the discussion in Section 3.1 above. Variations in vertical profiles of the draped magnetic field in response to solar wind conditions will affect the distribution and intensity of ionospheric conductivity. On the day-side of Mars, this magnetic effect even appears to be stronger than the effects of variations in the electron density, which is stably provided by solar illumination. Thus global changes in the draping strength and geometry because of the changes in the IMF intensity and direction should have an immediate effect on the current systems evolving in this highly conducting ionosphere. We could thus foresee temporal variations—when the magnetic morphology changes in response to solar wind IMF forcing, leading to changes in ionospheric conductivities.

Furthermore we could foresee spatial gradients in regions where the conductivities decrease because of ceasing solar illumination (i.e. large SZA), which is noticeable at very high latitude regions close to the poles and/or the lower latitude terminators. Here strong day-side ionospheric currents will have to close, preferably via field-aligned currents or, if remaining in the horizontal plane, via new secondary horizontal current systems driven by induced electric fields.

Depending on the direction of the IMF, an effective flaring of the draped magnetic field-lines can occur close to the terminators. This obviously alters the exact way in which the magnetic field strength declines at the inner magnetospheric boundary, thereby changing the ionospheric conductivities in these regions. For any IMF direction along the sub-solar tangential plane (only Z or only Y direction in MSO coordinates), magnetically induced conductivity changes will therefore almost coincide with gradients in the solar photo-ionisation at the terminators. For more oblique solar wind IMF directions, the magnetospheric flaring will occur more towards the day- or night-side regions of the planet. Thus, again the solar wind will control the current flow around the planet in a very complicated interplay.

Even though ionospheric and field-aligned currents have to our knowledge not yet been observed on Mars, we expect that either solar wind or atmospheric drivers should easily excite strong currents in such a highly conducting ionosphere. Brain (2006) reports that at mid-latitudes, the day-side magnetic field observed by MGS is on average a factor of two or more stronger than on the night-side, with large increases in certain regions of the crustal sources. He concludes that this excess field on the day-side has most likely two sources, the draped IMF and the current generated magnetic fields.

4.2. Conductivities above strong crustal anomalies and consequences of strong day-side conductivity gradients

Strong field-aligned current flow at terminators and poles due to horizontal current divergence in regions of decreasing solar

illumination is a problem that probably exists at all planets and planet-like bodies with draped magnetospheres and an ionised upper atmosphere.

However, on Mars the situation is somewhat more complicated. We have shown in Section 3.2 that in regions above crustal magnetic anomalies the ionospheric conductivity is not only much weaker than in the undisturbed regions but it also reduces from a strong three-layer altitude profile to a weaker two-layer altitude profile, with a strong lower layer basically disappearing. Again the relative strength of the draped magnetosphere as compared to the magnetic field strength of the crustal anomaly will determine the exact conductivity difference, but nonetheless there should exist very strong conductivity gradients between the regions above such anomalies and the undisturbed areas. As we know from the aurora in Earth's polar ionosphere, strong localised conductivity gradients will undoubtedly lead to horizontal current divergence through field-aligned currents. In the case of insufficient supplies of current carriers (i.e. electrons and ions) in the coupled ionospheric, magnetospheric and solar wind plasma regimes, strong induced electric fields will occur, either counteracting such currents within the ionosphere itself or diverting them to other regions, where field-aligned currents can balance horizontal current divergence. Thus, we note that strong conductivity gradients, including the disappearance of a complete electron Pedersen layer at a low ionospheric altitude over crustal anomalies, must give rise to exciting electrodynamics on the Martian day-side, which may make it look even more exciting than the terrestrial auroral zones.

This should be true both in a more global sense for the two hemispheres, considering the concentration of anomalies in the southern hemisphere, and also on a more regional scale between localised areas of crustal anomalies and adjacent weakly magnetised areas.

At this point, we should also recall that for the purpose of this study, which was only meant to show the existence of Titan-like conductivity layers at least in parts of the Martian ionosphere, we have only considered the total value of the guiding magnetic field. But we know that the magnetic field over and around crustal anomalies exhibits complicated geometries like closed field-line loops in domes and arcades and open radial field-lines in the so-called cusps. The direction of the magnetic field will determine the direction of the anisotropic ionospheric conductivity tensor, as both the Hall and the Pedersen conductivities are perpendicular to the prevailing magnetic field.

It is of course premature to predict any three-dimensional current flow geometry from the data presented here, but in the presence of such extreme conductivity gradients it must be safe to postulate that open cusps of radial magnetic field between the more arcade- or dome-like geometries of crustal anomalies (Brain et al., 2003; Gurnett et al., 2008; Duru, 2006; Nielsen et al., 2007b) should provide ideal magnetic topologies for the three-dimensional closure of strong horizontal ionospheric currents, and efficient coupling to the surrounding IMF.

The magnetic loops of domes and arcades should also be susceptible to magnetic reconnection with the impinging solar wind IMF, resulting in dynamic rather than stationary cusp field-aligned currents. Any such field-aligned current system will most likely in turn also result in particle acceleration along the magnetic field-lines and other typical auroral phenomena, which have already been observed by Lundin et al. (2006), Bertaux et al. (2005), and Brain et al. (2006b) on the night-side of Mars.

A further degree of complication in Martian electrodynamics will be introduced by the fact that such conductivity gradients around the crustal anomalies will only be frozen to the magnetic structure on the central day-side of the planet, where the draped magnetic field is reasonably horizontal (with a well-developed inner boundary) and where the atmospheric ionisation is relatively homogeneous. As the anomalies rotate out of the day-side at the dusk terminator and back into it on the dawn terminator, the associated conductivity gradients and current systems will gradually develop and change, as Mars faces the solar wind with an ever changing, but nevertheless periodic, magnetic topology.

We summarise that future studies of the electrodynamics of Mars should take into account

- the variability in the global topology of the induced magnetosphere due to IMF intensity and direction (and possibly also the solar wind dynamic pressure) as it affects the local vertical profiles of magnetic field over the planet,
- the rotation of the actual planetary surface and the imbedded magnetic structures in relation to these external influences, and
- the local and global changes in ion production rate around the crustal anomalies and at the terminators and poles depending on solar illumination and other ionising sources like particle precipitation.

This will be an interesting but demanding enterprise.

4.3. Outlook for other planets

In this paper, we have shown that in regions of weakly magnetised crustal anomalies Mars behaves, in terms of ionospheric conductivities, very much like Titan, but very unlike Earth. In accordance with Rosenqvist et al. (2009), we conclude that the basic reason for this new three-layer vertical structure of conductivities is the decline in the induced magnetic field at its inner boundary, where a decrease in gyro-frequency allows a collisional electron conductivity layer. The basic requirement is that the altitude where $\Omega_e = \nu_e$ occurs should be in a region of reasonably strong ionisation. We find that these conditions are fulfilled at both Titan and Mars, for very different conditions of magnetic field draping, ionisation and composition of the upper atmosphere. They are seen to emerge at vastly different altitudes of around 1300 km for Titan and around 130 km for Mars. Nevertheless, we did find that the basic physics are similar in both cases.

It appears reasonable to assume that the extent to which an induced magnetosphere penetrates an underlying upper ionosphere, is determined by a balance of ionospheric quantities, such as temperature and electron density, (that is essentially the ionospheric thermal pressure from below) with the magnetic field pressure imposed from above. Thus we should expect to see similar conditions to those found on Titan and the northern hemisphere of Mars to exist also on Venus, other unmagnetized planet-like moons of the giant planets, and possibly even on comets. Just like for Titan and Mars, we have found that little has been written about the actual altitude dependence of ionospheric conductivities at such bodies. One of the few studies is by Cloutier and Daniell (1973), referring to altitude dependencies for the ratios of electron and ion conductances at Mars and Venus, correctly identifying the importance of the electron terms in the Pedersen conductivity. However, at Mars they stop their calculations at an altitude of 200 km, finding a ratio of 1. On Venus, they continue their calculations down to 100 km, finding that the electron term becomes dominant just below 200 km. Obviously, more refined data should exist at Venus today to verify their results below 200 km.

5. Conclusions

Rosenqvist et al. (2009) found that Titan's ionosphere is very conducting, at least one order of magnitude stronger than at Earth. On Titan, the structure of a draped magnetosphere was seen to give rise to three distinct layers of conductivity (2 Pedersen and 1 Hall layers). We postulated that the regions with cleanly draped magnetic field on Mars, or any other planet with an induced magnetosphere resulting from magnetic field line draping, should exhibit a similar ionospheric behaviour.

In our study for Mars we found that, indeed, such a conductivity profile prevails in large portions of the northern hemisphere of Mars where the crustal magnetization is negligible. We also induced the existence of different and more Earth-like conductivity profiles close to and above strong crustal magnetic anomalies. Thus we conclude that the electrodynamics of the Martian magnetosphere are characterized by the co-existence of a complicated combination of a time-varying draped magnetosphere (mostly above the northern hemisphere with three intense but variable, conductivity layers) and mini-magnetospheres, exhibiting domes and cusps close to strong crustal magnetic fields (mostly in the southern hemisphere where the conductivities are weaker and more Earth-like with mainly 2 layers). This should give rise to interesting and dynamic 3-dimensional current systems, most probably also involving field-aligned currents and aurorae at the resulting conductivity gradients. One can expect enhanced solar wind coupling along radial *B*-field components.

While the complicated co-existence of Titan- and Earth-like features is a specialty of Mars, we postulate that other planets and planet-like bodies with induced magnetospheres bordering ionised upper atmospheres might host similar three-layer conductivity conditions as Titan and the northern hemisphere of Mars.

Acknowledgements

HO is presently on a secondment for scientific research from ESA to the Swedish Institute of Space Physics (IRF) in Uppsala, Sweden. He acknowledges support for scientific work from the IRF in Sweden and the MPS and DLR in Germany. RSD, ML and SEM are supported by STFC grant PP/E000983/1. NJTE is supported through a grant from the Swedish Research Council (VR), PW acknowledges support from NASA's Mars Fundamental Research Program grant NNX08AN56G, and the work of DB is supported by NASA grant NNX06AD97G.

References

Acuña, M.H., Connerney, J.E.P., Wasilewski, P., Lin, R.P., Anderson, K.A., Carlson, C.W., McFadden, J., Curtis, D.W., Mitchell, D., Rème, H., Mazelle, C., Sauvaud, J.A., d'Uston, C., Cros, A., Medale, J.L., Bauer, S.J., Cloutier, P., Mayhew, M., Winterhalter, D., Ness, N.F., 1998. Magnetic field and plasma observations at mars: initial results of the mars global surveyor mission. Science 279, 1676–1680.

Acuña, M.H., Connerney, J.E.P, Wasilewski, P., Lin, R.P., Mitchell, D., Anderson, K.A., Carlson, C.W., McFadden, J., Reme, H., Mazelle, C., Vignes, D., Bauer, S.J., Cloutier, J.P., Ness, N.F., 2001. Magnetic field of Mars: Summary of results from the aerobraking and mapping orbits. J. Geophys. Res. 106, 23403–23418.

Banks, P.M., Kockarts, G., 1973. Aeronomy. *Academic Press*, New York, London.

Bertaux, J.L., F. Leblanc, O. Witasse, E. Quemerais, J. Lilensten, S.A. Stern,B. Sandel and O. Korablev, 2005, Discovery of an aurora on Mars, Nature, 435, 790-794.

Bertucci, C., Mazelle, C., Crider, D.H., Vignes, D., Acuña, M.H., Mitchell, D.L., Lin, R.P., Connerney, J.E.P., Réme, H., Cloutier, P.A., Ness, N.F., Winterhalter, D., 2003. Magnetic field draping enhancement at the Martian magnetic pileup boundary from Mars Global Surveyor observations. Geophys. Res. Lett. 30 (2), 1099, doi:10.1029/2002GL015713.

Boström, R., 1964. A model of the auroral electrojects. *J. Geophys. Res.* 69, 4983–4999.

Brain, D.A., 2006. Mars Global Surveyor Measurements of the Martian Solar Wind Interaction. Space Sci. Rev. 126, 77–112, doi:10.1007/s11214-006-9122.

Brain, D.A., F. Bagenal, M.H. Acuña, and J.E.P. Connerney (2003), Martian magnetic morphology: contributions from the solar wind and crust, J. Geophys. Res., 108, 10.1029/2002JA009482.

Brain, D.A., Halekas, J.S., Peticolas, L.M., Lin, R.P., Luhmann, J.G., Mitchell, D.L., Delory, G.T., Bougher, S.W., Acuña, M.H., Rème, H., 2006a. On the origin of aurorae on Mars. *Geophys. Res. Lett.* 33, L01201, doi:10.1029/2005GL024782.

Brain, D.A., Mitchell, D.L., Halekas, J.S., 2006b. The magnetic field draping direction at Mars from April 1999 through August 2004. Icarus 182, 464–473, doi:10.1016/j.icarus.2005.09.023.

Brain, D.A., Lillis, R.J., Mitchell, D.L., Halekas, J.S., Lin, R.P., 2007. Electron pitch angle distributions as indicators of magnetic field topology near Mars. *J. Geophys. Res.* 112, A09201, doi:10.1029/2007JA012435.

Cain, J.C., Ferguson, B.B., Mozzoni, D., 2003. An $n=90$ internal potential function of the Martian crustal magnetic field. J. Geophys. Res. 108 (E2), 5008, doi:10.1029/2000JE001487.

Chen, R.H., Cravens, T.E., Nagy, A.F., 1978. The martian ionosphere in light of the viking observations. J. Geophys, Res. 83, 3871.

Chicarro, A., Martin, P., Traunter, R., 2004. The Mars Express mission: an overview. In: Wilson, A. (Ed.), Mars Express: a European Mission to the Red Planet, SP-1240. European Space Agency Publication Division, Noordwijk, Netherlands, pp. 3–16.

Cloutier, P.A., Daniell, R.E., 1973. Ionospheric currents induced by solar wind interaction with planetary atmospheres. Planet. Space Sci. 21, 461–474.

Cowley, S.W.H., 2000. Magnetosphere-Ionosphere interaction: a tutorial review, Magnetospheric current systems. AGU Geophys. Monogr. Ser. 118, 91–106.

Connerney, J.E.P., Acuna, M.H., Wasilewski, P.J., Kletetschka, G., Ness, N.F., Reme, H., Lin, R.P., Mitchell, D.L., 2001. The global magnetic field of Mars and implications for crustal evolutions. Geophys. Res. Lett. 28, 4015–4018.

Dubinin, E., Chanteur, G., Fraenz, M., Woch, J., 2008. Field-aligned currents and parallel electric field potential drops at Mars. Scaling from the Earth's aurora. Planet. Space Sci. 56, 868–872.

Duru, F., 2006, Magnetically controlled structures in the ionosphere of Mars. MSc-Thesis. University of Iowa, IOWA, USA, July 2006.

Edberg, N.J.T., Lester, M., Cowley, S.W.H., Eriksson, A.I., 2008. Statistical analysis of the location of the Martian magnetic pileup boundary and bow shock and the influence of crustal magnetic fields. J. Geophys. Res. 113, A08206, doi:10.1029/2008JA013096.

Egedal, J., 1947. The magnetic diurnal variation of the horizontal force near the magnetic equator. Terr. Magn. Atmos. Electr. 52, 449–451.

Fox, J.L., Yeager, K.E., 2006. Morphology of the near-terminator Martian ionosphere: a comparison of models and data. *J. Geophys. Res.* 111, A10309.

Gurnett, D.A., Huff, R.L., Morgan, D.D., Persoon, A.M., Averkamp, T.F., Kirchner, D.L., Duru, F., Akalin, F., Kopf, A.J., Nielsen, E., Safaeinili, A., Plaut, J.J., Picardi, G., 2008. An overview of radar soundings of the martian ionosphere from the Mars Express spacecraft. Adv. Space Res. 41, 1335–1346.

Hanson, W.B., Sanatani, S., Zuccaro, D.R., 1977. The Martian ionosphere as observed by the Viking retarding potential analyzers. J. Geophys. Res. 82, 4351–4363, doi:10.1029/JS082i028p04351.

Kelley, M.C., 1989. The Earth's ionosphere, plasma physics and electrodynamics. International Geophysics Series, vol. 43. Academic Press, San Diego.

Luhmann, J.G., Brace, L.H., 1991. Near-Mars space. Rev. Geophys. 29, 121–140.

Lundin, R., et al., 2004. Solar wind-induced atmospheric erosion at Mars: first results from ASPERA-3 on Mars Express. Science 305, 1933.

Lundin, R., Winningham, D., Barabash, S., Frahm, R., Holmström, M., Sauvaud, J.A., Fedorov, A., Asamura, K., Coates, A.J., Soobiah, Y., Hsieh, K.C., Grande, M., Koskinen, H., Kallio, E., Kozyra, J., Woch, J., Fraenz, M., Brain, D., Luhmann, J., McKenna-Lawler, S., Orsini, R.S., Brandt, P., Wurz, P., 2006. Plasma acceleration above martian magnetic anomalies. Science 311, 980–983, doi:10.1126/science.1122071.

Mitchell, D.L., Lin, R.P., Mazelle, C., Reme, H., Cloutier, P.A., Connerney, J.E.P., Acuna, M.H., Ness, N.F., 2001. Probing Mars' crustal magnetic field and ionosphere with the MGS electron reflectometer. J. Geophys. Res. 106 (23419–23428), 2001.

Nagy, A.F., Winterhalter, D., Sauer, K., Cravens, T.E., Brecht, S., Mazelle, C., Crider, D., Kallio, E., Zakharov, A., Dubinin, E., Verigin, M., Kotova, G., Axford, W.I., Bertucci, C., Trotignon, J.G., 2004. The plasma environment of Mars. Space Sci. Rev. 111, 33–114, doi:10.1023/B:SPAC.0000032718.47512.92.

Nielsen, E., Morgan, DD., Kirchner, D.L., Plaut, J., Picardi, G., 2007a. Absorption and reflection of radio waves in the Martian ionosphere. Planet. Space Sci. 55, 864–870, doi:10.1016/j.pss.2006.10.005.

Nielsen, E., Wang, X.-D., Gurnett, D.A., Kirchner, D.L., Huff, R., Orosei, R., Safaeinili, A., Plaut, J.J., Picardi, G., 2007b. Vertical sheets of dense plasma in the topside Martian ionosphere. J. Geophys. Res. 112, E02003, doi:10.1029/2006JE002723.

Pätzold, M., Tellmann, S., Häusler, B., Hinson, D., Schaa, R., Tyler, G.L., 2005. A sporadic third layer in the ionosphere of Mars. Science 310 (no. 5749), 837–839.

Picardi, G., Biccari, D., Seu, R., et al., 2004. MARSIS: Mars advanced radar for subsurface and ionosphere sounding. In: Wilson, A. (Ed.), Mars Express: a European mission to the red planet, SP-1240. European Space Agency Publication Division, Noordwijk, Netherlands, pp. 51–70.

Purucker, M., Ravat, D., Frey, H., Voorhies, C., Sbaka, T., Acuna, M.H., 2000. An altitude normalized magnetic map of Mars and its interpretation. Geophys. Res. Lett. 27, 2449–2452.

Rosenqvist, L., Wahlund, J.E., Ågren, K., Modolo, R., Opgenoorth, H.J., Strobel, D., Mueller-Wodarg, I., Garnier, P., Pertucci, C., 2009. Titan ionospheric conductivities from Cassini measurements. Planet. Space Sci. 10, 1016.

Schunk, R.W., Nagy, A.F., 2000. Ionospheres.. Cambridge University Press, Cambridge, UK.

Tyler, G.L., Balmino, G., Hinson, D.P., Sjogren, W.L., Smith, D.E., Simpson, R.A., Asmar, S.W., Priest, P., Twicken, J.D., 2001. Radio science observations with Mars Global Surveyor: orbit insertion through one Mars year in mapping orbit. J. Geophys. Res. 106, 23327–23348.

Withers, P., 2008. Theoretical models of ionospheric electrodynamics and plasma transport. J. Geophys. Res. 113, A07301, doi:10.1029/2007JA012918.

Withers, P., 2009. A review of observed variability in the dayside ionosphere of Mars. *Adv. Space Res.* 44, 277–307.